ACS SENSORS

Letter

Cite This: ACS Sens. XXXX, XXX, XXX−XXX

pubs.acs.org/acssensors

Vibrational Sensing Using Infrared Nanoantennas: Toward the Noninvasive Quantitation of Physiological Levels of Glucose and Fructose

Lucca Kühner,[†] Rostyslav Semenyshyn,[†] Mario Hentschel,[†] Frank Neubrech,[†,§] Cristina Tarín,[∥] and Harald Giessen*[,†]

[†]4th Physics Institute and Research Center SCoPE, University of Stuttgart, Pfaffenwaldring 57, 70569 Stuttgart, Germany

[§]Kirchhoff Institute for Physics, University of Heidelberg, Im Neuenheimer Feld 227, 69120 Heidelberg, Germany

[∥]Institute for System Dynamics and Research Center SCoPE, University of Stuttgart, Waldburgstraße 17/19, 70563 Stuttgart, Germany

Supporting Information

ABSTRACT: Monosaccharides, which include the simple sugars such as glucose and fructose, are among the most important carbohydrates in the human diet. Certain chronic diseases, e.g., diabetes mellitus, are associated with anomalous glucose blood levels. Detecting and measuring the levels of monosaccharides in vivo or in aqueous solutions is thus of the utmost importance in life science, health, and point-of-care applications. Noninvasive sensing would avoid problems such as pain and potential infection hazards. Here, with the help of surface enhanced infrared absorption (SEIRA) spectroscopy, we demonstrate the reliable optical detection in the mid-infrared spectral range of pure glucose and fructose solutions as well as mixtures of both in aqueous solution. We utilize a reflection flow cell geometry with physiologically relevant concentrations as small as 10 g/L. As significant improvement over the standard baseline correction employed in SEIRA applications, we utilize principal component analysis (PCA) as machine learning algorithm, which is ideally suited for the extraction of vibrational data. We anticipate our results as important step in biosensing applications that will stimulate efforts to further improve the employed SEIRA substrates, the noise level of the spectroscopic light source, as well as the flow cell environment en route to significantly higher sensitivities and quantitative analysis, even in tear drops.

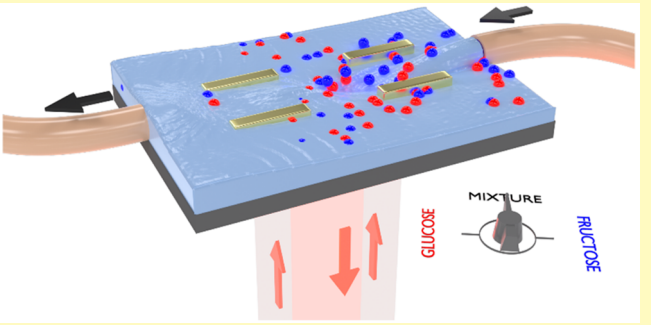

KEYWORDS: *glucose, fructose, glucose sensor, biosensing, surface-enhanced infrared absorption, principal component analysis, optical and noninvasive sensing*

Plasmonic sensors open up new routes in noninvasive optical sensing applications, such as gas sensing,[1,2] biomedical sensing,[3,4] and homeland security.[5] These sensors make use of the localized surface plasmon resonance (LSPR) in metallic nanoparticles[6,7] which is a collective oscillation of the quasi-free conduction electrons within the metal nanoparticle. The resonance position is mainly affected by geometrical parameters and, most importantly, by the surrounding refractive index.[8] Thereby, changes in the refractive index of the environment can be detected and attributed to the presence of a specimen.[9] As a logical consequence, the approach suffers from poor selectivity since substances with similar refractive indices cannot be differentiated using this method. Therefore, efforts have been made to combine the high sensitivity of refractive index sensing with the highly molecule-specific approach, such as infrared spectroscopy.[10]

In contrast to refractive index sensing, infrared spectroscopy (IR) enables material-specific identification of chemical species making use of their characteristic molecular vibrations in the mid-infrared (MIR) region.[11,12] However, the sensitivity of this approach is low, requiring large amounts of analyte due to the small molecular absorption cross sections. To overcome this sensitivity limitation, surface-enhanced infrared absorption (SEIRA) spectroscopy[13−19] is employed. Here, resonantly tuned metallic nanoantennas excited by an incoming light field transfer far-field energy into local nanoscale volumes, leading to highly enhanced local electromagnetic near-fields, the so-called *hot spots*.[20] Molecules located inside these hot spots will interact with the plasmonic nanoantenna via these local electromagnetic near-fields. Consequently, the molecular vibrations will manifest themselves in the far-field response of the nanoantenna as vibrational features on-top of the

Received: March 11, 2019
Accepted: May 7, 2019

DOI: 10.1021/acssensors.9b00488
ACS Sens. XXXX, XXX, XXX−XXX

plasmonic line shape. It has been shown that the enhancement factor of the vibrational features can be as large as 5−6 orders of magnitude.[14,21] This technique is consequently able to provide the required sensitivity and selectivity for the optical detection of biomolecular species, such as, e.g., glucose or fructose.

Glucose is an essential substance in the human metabolism. Consequently, anomalous glucose levels in the blood can indicate the emergence and existence of the chronic and incurable disease *diabetes mellitus*.[22,23] In fact, *diabetes mellitus* is caused by a severe malfunction of glucose regulation due to insufficient insulin supply[24] affecting an ever increasing number of patients worldwide.[25] As a result, sizable medical research is dedicated to glucose detection, measurement, and sensing,[26−28] as well as glucose regulation in the human blood,[29,30] which is said to be the key to most suitably treat the disease. Thus, a sensor which allows for a reliable and frequent observation of glucose levels is highly desirable. So far, existing glucose sensors either rely on an invasive detection principle[31] or are still in the state of development[32] or appear somewhat cumbersome.[33]

In this Letter, we present an optical approach for *noninvasive* glucose sensing based on the specificity and sensitivity of SEIRA spectroscopy. Our ansatz allows sensing of glucose concentrations in the human ocular fluid or interstitial fluid that can be directly correlated to the blood glucose concentrations.[34] Moreover, we introduce a mathematical algorithm known as principal component analysis (PCA)[35] for state-of-the-art data analysis. Apart from its intrinsic stability against dynamic changes in the sensor environment, the algorithm is independent of input parameters and thus completely objective and fully autonomous. We believe that the combination of SEIRA and PCA is uniquely suited for a new noninvasive sensor principle.

Our experimental scheme for reliable optical detection of different concentrations of aqueous glucose and fructose solutions is depicted in Figure 1. We utilize a reflection flow cell in inverse geometry which is flushed via attached tube connectors that transport the desired solutions into and out of the flow cell. The key parts of our sensor are the different linear gold antenna arrays which were fabricated with electron beam lithography (EBL) on top of IR transparent calcium fluoride substrates (see top right panel of Figure 1). The geometrical parameters of the nanoantennas, such as the length L, height h, and width w, are chosen such as to exhibit a plasmon resonance at the spectral position of the targeted molecular vibrations of glucose and fructose. Following this approach, the gold antenna length is 3500 nm with a width and thickness of 100 nm, with a 2 nm chromium adhesion layer underneath. The periodicity is 4500 nm in x direction and 3000 nm in y direction. Hence, the local near-field strength and thus the coupling to the molecular vibrations is further increased by adjusting the transversal spacing between the nanoantennas such that the plasmon resonance spectrally coincides with the Rayleigh anomaly.[36,37] To optically probe the sensor, a commercial FTIR spectrometer (Bruker VERTEX 80) coupled to an optical microscope (Bruker Hyperion 2000, Schwarzschild objective with 15-fold magnification, NA = 0.4) is utilized. As indicated in the setup sketch, the IR radiation (globar) impinges from the back side of the sensor where it is focused onto the gold nanoantenna array. Here, the incoming IR light field excites the plasmonic modes in the nanoantenna array. The local electric near-field mediates the coupling of the

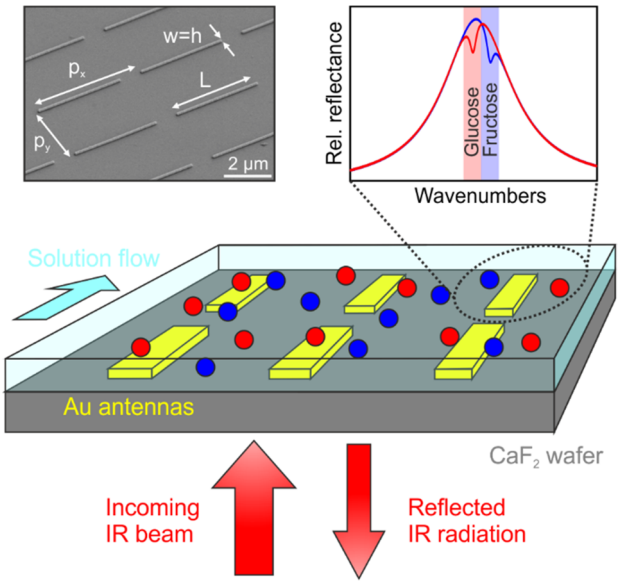

Figure 1. Measurement principle and sensor design. Arrays of linear gold nanoantennas (top left panel) are fabricated with electron beam lithography on top of an IR transparent CaF_2 wafer. Mixtures of aqueous glucose and fructose solutions (molecules indicated as red and blue spheres) are flushed into the flow cell via tube connectors. Our sensor is probed by a commercial FTIR setup coupled to an optical microscope which focuses an IR beam impinging from the backside. The reflected SEIRA signal is referenced to a gold mirror. The spectra, here schematically illustrated in the top right panel, allow for the noninvasive discrimination of glucose and fructose due to their characteristic vibrational bands in the mid-infrared.

plasmonic resonance with the vibrational modes of the molecules. Thus, the nanoantennas are reporting this enhanced vibrational fingerprint to the far-field present as narrowband Fano resonance signature encoded in the antenna scattering spectrum.[38] The spectra are measured with a nitrogen-cooled mercury cadmium telluride (MCT) detector and referenced to a gold mirror.

As a first important step, we study the response of our sensor to pure glucose and fructose solutions, shown in Figure 2a and b, respectively. For both solutions the concentration is 50 g/L. The acquired SEIRA reflectance spectra show the broad spectral signature of the plasmonic resonance. On top of this resonant feature, we can clearly identify vibrational signatures, which coincide with the known vibrational bands of glucose and fructose, as indicated by the red and blue bars. The acquired spectra are composed of both the plasmon resonance and the enhanced vibrational signals, which can be seen even better in the insets in panels (a) and (b). These signals exhibit a Fano line shape due to the molecular-plasmonic coupling. However, the Fano line shape is quite symmetric, rather Lorentzian, which is caused by the almost perfect coupling between the plasmonic and the vibrational mode due to the energetic degeneracy $\omega_{vib} \approx \omega_{plas}$.

To decouple the two contributions and to extract the vibrational signal, a standard baseline-correction routine is employed.[39,40] The idea behind baseline-correction is to reconstruct the unperturbed plasmon resonance signature and thus be able to remove it from the spectra. The corresponding baselines for the glucose and fructose measurements are indicated as black dashed lines overlaid with the measured data in Figure 2a and b. By dividing the SEIRA

DOI: 10.1021/acssensors.9b00488
ACS Sens. XXXX, XXX, XXX−XXX

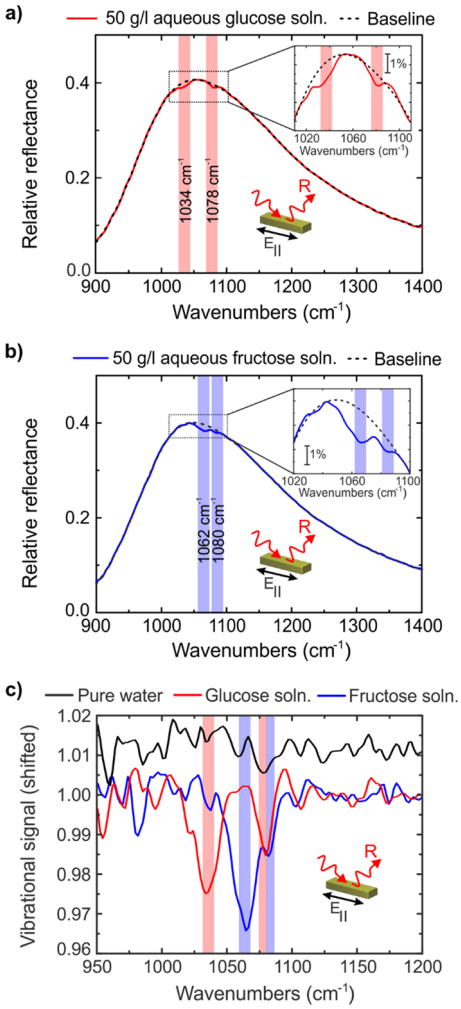

Figure 2. SEIRA spectra of aqueous glucose and fructose solutions. (a) SEIRA reflectance spectra of a c = 50 g/L aqueous glucose solution acquired in parallel polarization. (b) Same for fructose. The molecular vibrations are highlighted by the bars. The baseline as obtained from the baseline-correction procedure is overlaid with the measured data as black dashed line (see also inset). (c) Baseline-corrected vibrational spectra of pure aqueous water environment in the flow cell (black line) and a c = 50 g/L aqueous fructose solution (blue line) as well as a c = 50 g/L aqueous glucose solution (red line). The two monosaccharides are clearly distinguishable by their SEIRA spectrum.

spectrum by the reconstructed baseline, the spectra can be decomposed, and the purely enhanced vibrational spectra as depicted in Figure 2c are obtained. For comparison, a shifted baseline-corrected spectrum of a pure water environment is depicted in addition to the c = 50 g/L aqueous glucose and fructose environment within the flow cell. Apparently, water shows no vibrational peaks in the spectral region of interest, this excludes the possibility that a vibrational peak of the solutions originates from the water itself.

By comparing the baseline-corrected spectra of the two monosaccharides, it is straightforward to differentiate them solely by their SEIRA spectrum. Apart from the overlapping vibrational bands of fructose and glucose around 1080 cm^{-1}, a characteristic glucose vibration appears at 1034 cm^{-1} and analogous for fructose at 1062 cm^{-1}. In the following, these characteristic fingerprint vibrations are used to sense and discriminate glucose from fructose.

As a demonstration of our sensor principle, cycles of pure aqueous glucose and pure aqueous fructose solutions of varying concentration have been measured and are shown in the Supporting Information (SI) Figures S1 and S2. The measurements demonstrate the reliable detection of glucose and fructose down to a concentration of c = 10 g/L = 55 mM, which is close to the glucose concentrations for diabetes patients in the range from 2 to 40 mM in the human blood and from 2 to 22 mM in the interstitial fluid.[34] The measurements also show that the concentration limit can be further decreased by appropriate sensor design and data analysis. We are utilizing rod nanoantennas as the basic plasmonic building block. However, more complex geometries might further increase the local near-field enhancement or the volume of the enhanced field strength and thus the number of molecules sensed.

Most sensors are highly prone to crosstalk of other chemical species besides the ones of interest. This is particularly true for purely refractive index shift-based sensors such as unfunctionalized plasmonic nanoantennas.[9] Our sensor concept, however, can distinguish chemically very similar compounds by their vibrational fingerprints, as evidenced by the measurement in Figure 2 for the highly relevant case of glucose and fructose. As further proof of the superior sensor performance we now analyze mixed aqueous solutions of glucose and fructose of varying concentrations and mixing ratios, shown in Figure 3. All spectra are obtained from the identical nanoantenna array. The solutions are flushed through the flow cell, alternating with pure water purging solutions.

For a systematical study, we perform a measurement cycle and flush the flow cell with the corresponding mixture for each step. In between two different concentrations, the cell is flushed with pure water to remove precipitated residues of the solute or dirt. The measurement routine is depicted in the upper part of Figure 3, giving the respective concentration of

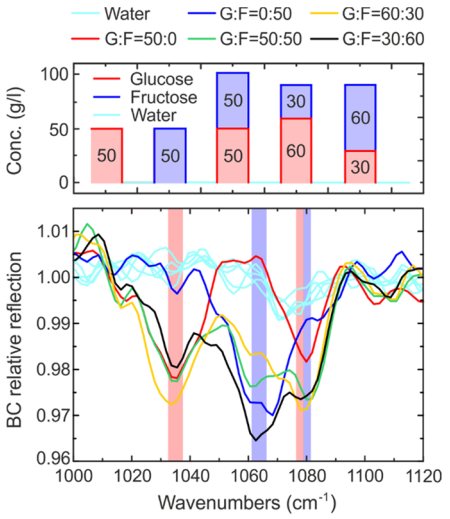

Figure 3. Baseline-corrected (BC) vibrational spectra of mixed aqueous fructose and glucose solutions. The top panel illustrates the measurement cycle with mixed aqueous glucose and fructose solutions. Here, the blue bars indicate the fructose concentrations (g/l) and the red bars the glucose concentrations (g/l). For the stacked bars, the total sugar concentrations add up. The bottom panel shows the corresponding baseline-corrected vibrational reflectance spectra for each measurement step of the cycle with the respective concentrations given on top of the figure. It is rather difficult to derive quantitative results from the baseline-corrected spectra.

DOI: 10.1021/acssensors.9b00488
ACS Sens. XXXX, XXX, XXX−XXX

glucose by the red and fructose by the blue bars. Starting from a pure aqueous glucose solution and followed by a pure aqueous fructose solution of 50 g/L each, an equal mixture of aqueous glucose and fructose (50 g/L and 50 g/L) is flushed into the flow cell. Afterward, the cycle is completed by a (60 to 30 g/L) and a (30 to 60 g/L) aqueous (glucose to fructose) mixture. For each measurement step, SEIRA spectra are taken in reflection and referenced to a gold mirror. Performing a baseline correction routine, we extract the enhanced vibrational signal for each measurement, shown in the lower panel of Figure 3. As a guide to the eye, the molecular vibrations of glucose are highlighted with red bars and those of fructose with blue bars.

The pure glucose (red curve) and fructose (blue curve) measurements show each only the vibrational modes of the corresponding analyte, as expected. For the mixed solutions one can identify the vibrational modes of glucose and fructose. Also, the measurements for pure water show no vibrational signatures, demonstrating that the analytes are not precipitating or sticking to the sensor chip. Inspecting the spectra closely, the different pure solutions and also the different mixtures can be clearly distinguished.

However, from these measurements it is indicated that the baseline corrected spectra are not ideally suited for an automated and input parameter free evaluation in order to extract *quantitative information* about the respective concentration. In fact, this is caused by a number of issues. For each measurement cycle, the input parameters for the baseline-correction algorithm need to be adjusted in order to describe the unperturbed plasmon resonance correctly. This results in limited reproducibility when considering two different measurement cycles. In fact, this issue becomes visible when comparing the vibrational signals of the pure c = 50 g/L glucose and fructose solutions from the measurement cycle shown in Figure 3 with the measurements shown in Figure 2c. A difference of more than 0.5% of the vibrational signals is present, originating from different baseline-correction parameters. This issue is minor in case a substance is just supposed to be detected or identified. However, for a quantitative measurement, that is, for the determination of a concentration, it is critical to retrieve the exact values. Additionally, potential misinterpretations might arise when examining the baseline-corrected spectra for the mixed solutions, shown as black (30:60 g/L), yellow (60:30 g/L), and green (50:50 g/L) curve in the bottom panel of Figure 3. For example, the vibrational signal of the equal (50:50 g/L) mixture of glucose and fructose (green curve) exhibits a different vibrational signal at the fructose band at 1062 cm^{-1} compared to the pure aqueous fructose solution of similar concentration. Although the fructose concentrations are equal, the vibrational signals seemingly deviate from one another. However, as the vibrational signals of the pure glucose solution and the (50:50 g/L) mixture match, we ascribe this issue to an error in the baseline-correction procedure. These observations clearly underline that an evaluation method is required which is free of input parameters in order to allow for *quantitative* measurements.

Evaluating sensor data, in particular sequences of different measurement as in our case, relies on the identification of common patterns. The presence of, e.g., glucose in the solution, is associated with the presence of the corresponding vibrational fingerprints as well as a resonance shift due to a different effective refractive index. So far, we have identified these patterns manually by inspection of the baseline-corrected spectra. As we have seen, this becomes very difficult as soon as several vibrational bands are present which might even be of small modulation due to small concentrations.

The field of machine learning and data mining has become highly important over the past years due to ever increasing amount of data and the necessity to analyze and identify the content. In fact, significant efforts are invested in identifying patterns and similarities in these data sets.

Mathematically speaking, these problems are all very similar and are basically an eigenvector−eigenvalue problem. If common patterns are present within all data sets, represented as vector quantities, the overall data set can be represented as a linear combination of a limited set of eigenvectors. In our case, this is intuitively clear: All measurements of solutions containing, e.g., glucose will exhibit the vibrational bands of glucose (determined by an eigenvector) of varying intensity (determined by an eigenvalue). This evaluation method is called principal component analysis (PCA) and has become a standard tool in data analysis and data mining.

In detail, PCA decomposes the measured data and represents them in an orthogonal and uncorrelated set of eigenfunctions called principal components (PCs) and eigenvalues which are termed scores (SCs). Each term of the linear expansion is composed of the product of the PC as an eigenvector and a spectrum-specific score SC. Together with the average A of all measured spectra (in our case 300 spectra in total, 30 spectra for each of the ten measurement steps), each measured spectrum which is a 1D vector composed of 3502 channels can be described as follows

$$\text{spectrum}_i = A + \sum_{j=1}^{300} \text{SC}_{i,j} \cdot \text{PC}_j$$

The utilized algorithm determines the PCs such that the first one contributes the highest variance and thus constitutes the largest contribution. Analogously, the second order PC makes the second largest contribution and so forth. The correlation between individual data sets is more significant when fewer PCs are needed in order to describe the entire data set.

The first two PCs of our data set are displayed in Figure 4a. It is important to note that the PCs, as calculated by the algorithm, have no *a priori* physical interpretation. As they are supposed to capture the common patterns in the measurement and thus the physical processes, they are, however, expected to relate to a physical interpretation. Importantly, at this point it is not necessary to assign such a physical interpretation as the algorithm does not require any starting input at all. Figure 4b depicts the first and second order scores for all 300 measurements, color coded for each of the 30 measurements per fructose/glucose solution cycle. The data forms clear and very distinct clusters. The different solutions can be clearly separated and identified in the 2D space of the first and second order scores. In strong contrast to the impression left by the baseline corrected vibrational spectra shown in Figure 3b, the relative and absolute concentrations are well encoded into the first and second order scores. The clusters are well separated, which should also allow for the identification of intermediate concentration ratios as well as significantly smaller overall concentrations. For smaller concentrations, the data points are expected to shift closer to the pure water measurements on the right-hand side until they merge and become indistinguishable. However, it is obvious that there seems to be significant room

DOI: 10.1021/acssensors.9b00488
ACS Sens. XXXX, XXX, XXX−XXX

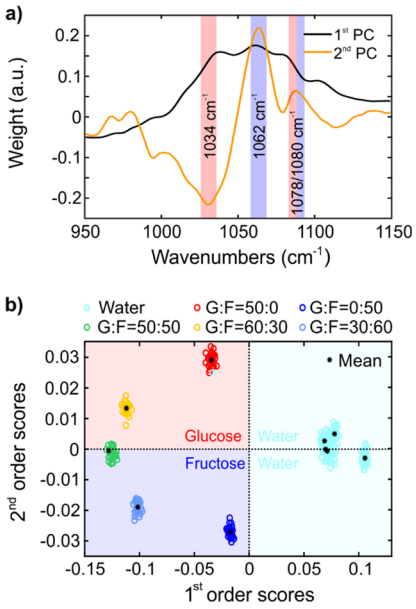

Figure 4. PCA analysis of mixed aqueous glucose and fructose solutions. (a) First and second principal component as obtained from PCA of our measurement cycle. The first component represents the spectral shift of the plasmonic resonance due to different effective refractive indices, whereas the second component comprises the vibrational information as also highlighted by the color-coded bars. (b) Plotting the corresponding second order score vs first order score for each measurement reveals clusters for each measurement step. The characteristic positions as obtained from the input parameter independent algorithm can be addressed to specific concentrations by calibrations measurements.

for the detection of smaller concentrations. For very small concentrations the vibrational fingerprints which are imprinted onto the spectra seem to vanish into the measurement noise. However, we believe, as underpinned by the PCA analysis shown in Figure 4b, that these features can in fact still be retrieved from the data by the PCA algorithm.

As mentioned before, the PCA evaluation of the measurements does not require any input parameters or any knowledge about the physical processes involved. Nevertheless, Figure 4b conclusively demonstrates the ability of the PCA algorithm to extract the different concentrations of the solutions, which is a crucial ingredient for an automated evaluation routine. However, indeed a physical interpretation can be assigned to the PCs in our case: The first PC takes the form of a resonance peak roughly coinciding with the plasmonic resonance of our antenna array. By adding (positive score value) or subtracting (negative score value) this feature from the average spectrum, the spectrum is blue-shifted or red-shifted, respectively. The first PC therefore captures the plasmonic resonance shift due to the different effective refractive indices of the solutions. In the case of the pure water solutions with the smallest effective refractive index, the plasmon resonance is furthest blue-shifted. For the solution with the largest overall glucose/fructose content of 100 g/L, the resonance is furthest red-shifted. The *x*-axis of our diagram is thus displaying the response of a pure refractive index sensor. It is clear that the first PC is not able to distinguish between solutions with the same/similar overall concentrations, as fructose and glucose yield the same refractive index shift at identical concentrations. Inspecting Figure 4a, we find that the second PC contains the vibrational information. As can be seen by the glucose and fructose vibrational bands highlighted in the Figure 4a, all four vibrational signatures are encoded in the second PC. This fact can also be seen in Figure 4b: The corresponding second order score plotted on the *y*-axis lifts the degeneracy of the first PC and allows for the discrimination of glucose from fructose. The vibrational bands of glucose and fructose have opposite signs, and thus the sign of the score values (and also their magnitude) encodes the molecular specificity. The feature is somewhat more complicated when compared to the refractive index shift encoded in the first PC as glucose and fructose have vibrational bands spectrally close at 1078 and 1080 cm^{-1}, respectively, which are superimposed into one feature. In order to further demonstrate the power of PCA, we have also evaluated the concentration dependent measurements of the pure aqueous solutions. The results are presented in Figures S3 and S4 in the Supporting Information.

In conclusion, we have demonstrated a noninvasive sensor principle which relies on the sensitivity and specificity provided by SEIRA. Within our work, we were able to achieve a sensitivity down to c = 10 g/L for pure aqueous fructose and glucose solutions which can easily be enhanced by utilizing a more sensitive sensing geometry, such as split-ring resonators or a more powerful light source, e.g., a quantum cascade laser as already demonstrated in previous works.[41−43] In addition, we demonstrated that the PCA algorithm is ideally suited for the evaluation of the sensor data to retrieve absolute glucose and fructose concentrations even within mixed solutions. We believe that the combination of SEIRA and PCA approach might lay the foundations for future noninvasive optical sensing that combines refractive index sensing and vibrational information down to extremely small physiological concentrations, as found, for example, in tear drops.

■ ASSOCIATED CONTENT

Supporting Information

The Supporting Information is available free of charge on the ACS Publications website at DOI: 10.1021/acssensors.9b00488.

Baseline-corrected data and PCA of pure glucose and fructose solutions down to a sensing limit of c = 10 g/L (PDF)

■ AUTHOR INFORMATION

Corresponding Author

*E-mail: Giessen@physik.uni-stuttgart.de.

ORCID

Rostyslav Semenyshyn: 0000-0001-6818-7500
Mario Hentschel: 0000-0002-6882-4183
Frank Neubrech: 0000-0002-5437-4118

Notes

The authors declare no competing financial interest.

■ ACKNOWLEDGMENTS

The authors gratefully acknowledge financial support by the ERC Advanced Grant (COMPLEXPLAS), Deutsche Forschungsgemeinschaft (SPP1839), Baden-Württemberg Stiftung (PROTEINSENS), MWK Baden-Württemberg (IQST, ZAQuant), BMBF.

DOI: 10.1021/acssensors.9b00488
ACS Sens. XXXX, XXX, XXX−XXX

REFERENCES

(1) Liu, N.; Tang, M. L.; Hentschel, M.; Giessen, H.; Alivisatos, A. P. Nanoantenna-Enhanced Gas Sensing in a Single Tailored Nanofocus. *Nat. Mater.* **2011**, *10* (8), 631−636.

(2) Tittl, A.; Mai, P.; Taubert, R.; Dregely, D.; Liu, N.; Giessen, H. Palladium-Based Plasmonic Perfect Absorber in the Visible Wavelength Range and Its Application to Hydrogen Sensing. *Nano Lett.* **2011**, *11* (10), 4366−4369.

(3) Brolo, A. G. Plasmonics for Future Biosensors. *Nat. Photonics* **2012**, *6* (11), 709−713.

(4) Jain, P. K.; Huang, X.; El-Sayed, I. H.; El-Sayed, M. A. Noble Metals on the Nanoscale: Optical and Photothermal Properties and Some Applications in Imaging, Sensing, Biology, and Medicine. *Acc. Chem. Res.* **2008**, *41* (12), 1578−1586.

(5) Qu, W.-G.; Deng, B.; Zhong, S.-L.; Shi, H.-Y.; Wang, S.-S.; Xu, A.-W. Plasmonic Resonance Energy Transfer-Based Nanospectroscopy for Sensitive and Selective Detection of 2,4,6-Trinitrotoluene (TNT). *Chem. Commun.* **2011**, *47* (4), 1237−1239.

(6) Enoch, S.; Bonod, N. *Plasmonics*; Springer series in optical sciences; Springer, 2012; Vol. *167*.

(7) Luk'yanchuk, B.; Zheludev, N. I.; Maier, S. A.; Halas, N. J.; Nordlander, P.; Giessen, H.; Chong, C. T. The Fano Resonance in Plasmonic Nanostructures and Metamaterials. *Nat. Mater.* **2010**, *9* (9), 707−715.

(8) Sherry, L. J.; Chang, S.-H.; Schatz, G. C.; Van Duyne, R. P.; Wiley, B. J.; Xia, Y. Localized Surface Plasmon Resonance Spectroscopy of Single Silver Nanocubes. *Nano Lett.* **2005**, *5* (10), 2034−2038.

(9) Liu, N.; Mesch, M.; Weiss, T.; Hentschel, M.; Giessen, H. Infrared Perfect Absorber and Its Application As Plasmonic Sensor. *Nano Lett.* **2010**, *10* (7), 2342−2348.

(10) Shih, W. C.; Santos, G. M.; Zhao, F.; Zenasni, O.; Arnob, M. M. P. Simultaneous Chemical and Refractive Index Sensing in the 1−2.5 Mm near-Infrared Wavelength Range on Nanoporous Gold Disks. *Nano Lett.* **2016**, *16* (7), 4641−4647.

(11) Griffiths, P. R. Infrared and Raman Instrumentation for Mapping and Imaging. In *Infrared and Raman Spectroscopic Imaging*; Wiley-VCH Verlag GmbH & Co. KGaA: Weinheim, Germany, 2009; pp 1−64.

(12) Griffiths, P. R.; de Haseth, J. *Fourier Transform Infrared Spectrometry*; John Wiley & Sons, Inc.: Hoboken, NJ, USA, 2007.

(13) Ataka, K.; Stripp, S. T.; Heberle, J. Surface-Enhanced Infrared Absorption Spectroscopy (SEIRAS) to Probe Monolayers of Membrane Proteins. *Biochim. Biophys. Acta, Biomembr.* **2013**, *1828* (10), 2283−2293.

(14) Neubrech, F.; Huck, C.; Weber, K.; Pucci, A.; Giessen, H. Surface-Enhanced Infrared Spectroscopy Using Resonant Nanoantennas. *Chem. Rev.* **2017**, *117* (7), 5110−5145.

(15) Kühner, L.; Hentschel, M.; Zschieschang, U.; Klauk, H.; Vogt, J.; Huck, C.; Giessen, H.; Neubrech, F. Nanoantenna-Enhanced Infrared Spectroscopic Chemical Imaging. *ACS Sensors* **2017**, *2* (5), 655−662.

(16) Rodrigo, D.; Limaj, O.; Janner, D.; Etezadi, D.; Garcia de Abajo, F. J.; Pruneri, V.; Altug, H. Mid-Infrared Plasmonic Biosensing with Graphene. *Science* **2015**, *349* (6244), 165−168.

(17) Wang, T.; Nguyen, V. H.; Buchenauer, A.; Schnakenberg, U.; Taubner, T. Surface Enhanced Infrared Spectroscopy with Gold Strip Gratings. *Opt. Express* **2013**, *21* (7), 9005.

(18) Kundu, J.; Le, F.; Nordlander, P.; Halas, N. J. Surface Enhanced Infrared Absorption (SEIRA) Spectroscopy on Nanoshell Aggregate Substrates. *Chem. Phys. Lett.* **2008**, *452* (1−3), 115−119.

(19) Adato, R.; Altug, H. In-Situ Ultra-Sensitive Infrared Absorption Spectroscopy of Biomolecule Interactions in Real Time with Plasmonic Nanoantennas. *Nat. Commun.* **2013**, *4*, 2154.

(20) Giannini, V.; Fernández-Domínguez, A. I.; Heck, S. C.; Maier, S. A. Plasmonic Nanoantennas: Fundamentals and Their Use in Controlling the Radiative Properties of Nanoemitters. *Chem. Rev.* **2011**, *111*, 3888−3912.

(21) Neubrech, F.; Pucci, A.; Cornelius, T. W.; Karim, S.; García-Etxarri, A.; Aizpurua, J. Resonant Plasmonic and Vibrational Coupling in a Tailored Nanoantenna for Infrared Detection. *Phys. Rev. Lett.* **2008**, *101* (15), 157403.

(22) Alberti, K. G. M. M.; Zimmet, P. Z. Definition, Diagnosis and Classification of Diabetes Mellitus and Its Complications. Part 1: Diagnosis and Classification of Diabetes Mellitus. Provisional Report of a WHO Consultation. *Diabet. Med.* **1998**, *15* (7), 539−553.

(23) Edelman, S. V. Importance of Glucose Control. *Med. Clin. North Am.* **1998**, *82*, 665−687.

(24) American Diabetes Association, A. D. Diagnosis and Classification of Diabetes Mellitus. *Diabetes Care* **2014**, *37*, S81−90.

(25) Ritz, E.; Rychlík, I.; Locatelli, F.; Halimi, S. End-Stage Renal Failure in Type 2 Diabetes: A Medical Catastrophe of Worldwide Dimensions. *Am. J. Kidney Dis.* **1999**, *34* (5), 795−808.

(26) Mesch, M.; Zhang, C.; Braun, P. V.; Giessen, H. Functionalized Hydrogel on Plasmonic Nanoantennas for Noninvasive Glucose Sensing. *ACS Photonics* **2015**, *2* (4), 475−480.

(27) Alexeev, V. L.; Das, S.; Finegold, D. N.; Asher, S. A. Photonic Crystal Glucose-Sensing Material for Noninvasive Monitoring of Glucose in Tear Fluid. *Clin. Chem.* **2004**, *50* (12), 2353−2360.

(28) Lee, Y.-J.; Pruzinsky, S. A.; Braun, P. V. Glucose-Sensitive Inverse Opal Hydrogels: Analysis of Optical Diffraction Response. *Langmuir* **2004**, *20* (8), 3096−3106.

(29) Vigersky, R. A.; Fonda, S. J.; Chellappa, M.; Walker, M. S.; Ehrhardt, N. M. Short- and Long-Term Effects of Real-Time Continuous Glucose Monitoring in Patients with Type 2 Diabetes. *Diabetes Care* **2012**, *35* (1), 32−38.

(30) García-Jaramillo, M.; Calm, R.; Bondia, J.; Tarín, C.; Vehí, J. Insulin Dosage Optimization Based on Prediction of Postprandial Glucose Excursions under Uncertain Parameters and Food Intake. *Comput. Methods Programs Biomed* **2012**, *105* (1), 61−69.

(31) Schulman, J. H., III; Whitmoyer, D. I. *Glucose Sensor Assembly*, August 26, 1997.

(32) Pleitez, M. A.; Hertzberg, O.; Bauer, A.; Seeger, M.; Lieblein, T.; Lilienfeld-Toal, H. v.; Mäntele, W. Photothermal Deflectometry Enhanced by Total Internal Reflection Enables Non-Invasive Glucose Monitoring in Human Epidermis. *Analyst* **2015**, *140* (2), 483−488.

(33) Tierney, M. J.; Tamada, J. A.; Potts, R. O.; Jovanovic, L.; Garg, S. Clinical Evaluation of the GlucoWatch® Biographer: A Continual, Non-Invasive Glucose Monitor for Patients with Diabetes. *Biosens. Bioelectron.* **2001**, *16* (9−12), 621−629.

(34) Bruen, D.; Delaney, C.; Florea, L.; Diamond, D. Glucose Sensing for Diabetes Monitoring: Recent Developments. *Sensors* **2017**, *17* (8), 1866.

(35) Abdi, H.; Williams, L. J. Principal Component Analysis. *Wiley Interdiscip. Rev. Comput. Stat.* **2010**, *2* (4), 433−459.

(36) Adato, R.; Yanik, A. A.; Wu, C.-H.; Shvets, G.; Altug, H. Radiative Engineering of Plasmon Lifetimes in Embedded Nanoantenna Arrays. *Opt. Express* **2010**, *18* (5), 4526.

(37) Bagheri, S.; Weber, K.; Gissibl, T.; Weiss, T.; Neubrech, F.; Giessen, H. Fabrication of Square-Centimeter Plasmonic Nanoantenna Arrays by Femtosecond Direct Laser Writing Lithography: Effects of Collective Excitations on SEIRA Enhancement. *ACS Photonics* **2015**, *2* (6), 779−786.

(38) Fano, U. Effect of Configuration Interaction on Intensities and Phase Shifts. *Phys. Rev.* **1961**, *124*, 1866−1878.

(39) Eilers, P. H. C.; Boelens, H. F. M. Baseline Correction with Asymmetric Least Squares Smoothing. *Life Sci.* **2005**, 1−26.

(40) Eilers, P. H. C. A. Perfect Smoother. *Anal. Chem.* **2003**, *75* (14), 3631−3636.

(41) Kröger, N.; Egl, A.; Engel, M.; Gretz, N.; Haase, K.; Herpich, I.; Kränzlin, B.; Neudecker, S.; Pucci, A.; Schönhals, A.; et al. Quantum Cascade Laser−based Hyperspectral Imaging of Biological Tissue. *J. Biomed. Opt.* **2014**, *19* (11), 111607.

(42) Schönhals, A.; Tholl, H.; Glasmacher, M.; Kröger-Lui, N.; Pucci, A.; Petrich, W. Optical Properties of Porcine Dermis in the Mid-Infrared Absorption Band of Glucose. *Analyst* **2017**, *142* (8), 1235−1243.

DOI: 10.1021/acssensors.9b00488
ACS Sens. XXXX, XXX, XXX−XXX

(43) Isensee, K.; Müller, N.; Pucci, A.; Petrich, W. Towards a Quantum Cascade Laser-Based Implant for the Continuous Monitoring of Glucose. *Analyst* **2018**, *143*, 6025.

DOI: 10.1021/acssensors.9b00488
ACS Sens. XXXX, XXX, XXX−XXX